SUMOylation of S100A10 promotes its nuclear localization and enhances the migration and invasion of PGCCs and their daughter cells

Qi Zhao
Tianjin People's Hospital Tianjin Union Medical Center
Kexin Zhang
Tianjin People's Hospital Tianjin Union Medical Center
Zugui Li
Tianjin People's Hospital Tianjin Union Medical Center
Hao Zhang
Tianjin People's Hospital Tianjin Union Medical Center
Fangmei Fu
Tianjin People's Hospital Tianjin Union Medical Center
Minying Zheng
Tianjin People's Hospital Tianjin Union Medical Center
Shiwu Zhang (zhangshiwu666@aliyun.con)
Tianjin People's Hospital Tianjin Union Medical Center https://orcid.org/0000-0002-5052-2283

Research

Keywords: S100A10, polyploidy giant cancer cells, SUMOylation, colorectal cancer, cell infiltration and migration

Posted Date: January 19th, 2021

DOI: https://doi.org/10.21203/rs.3.rs-147843/v1

Abstract

Background

Our previous studies have confirmed that cobalt chloride ($CoCl_2$) or chemoradiotherapy could induce the formation of polyploid tumor giant cells (PGCCs) and daughter cells derived from PGCCs had strong proliferation and migration abilities. However, the detailed molecular mechanism is unclear.

Methods

Cell functional experiments, co-immunoprecipitation, MG132 and ginkgolic acid treatment, western blot, and ChiP-Seq were used to identify the mechanism of S100A10 nuclear location.

Results

$CoCl_2$ was used to induce the formation of PGCCs in LoVo and HCT116 CRC cells. The proliferation and migration abilities of PGCCs and their daughter cells decreased significantly after S100A10 knockdown. In the control cells, S100A10 was mainly ubiquitinated, while in PGCCs and daughter cells, S100A10 was mainly SUMOylated, which was associated with S100A10 nuclear location. After SUMO1 was inhibited, the nuclear S100A10 in PGCCs and daughter cells decreased, and their proliferation and migration abilities significantly decreased. ChiP-Seq combined with real-time fluorescent quantitative PCR showed that S100A10 regulated the expression of neutrophil defensin 3 (*DEFA3*), receptor-type tyrosine-protein phosphatase N2 (*PTPRN2*), and rho guanine nucleotide exchange factor 18 (*ARHGEF18*). The expression of S100A10 in the nuclei and cytoplasm of rectal cancer after neoadjuvant chemoradiation (nCRT) and liver metastases increased compared with that in rectal cancer without nCRT.

Conclusion

The expression and nuclear localization of S100A10 modified by SUMOylation were associated with the high proliferation and migration of PGCCs and their daughter cells, and the differentiation, metastases, and relapse of CRCs by regulating the expression of *ARHGEF18*, *PTPRN2*, and *DEFA3*.

Background

PGCCs had the properties of cancer stem cells, and exhibited high resistance to hypoxia and chemotherapeutic drugs [1–5] and produced daughter cells via asymmetric cell division. Daughter cells derived from PGCCs expressed epithelial-mesenchymal transition-related proteins [5]. We have previously reported that irradiation or chemical reagents induced the formation of PGCCs and their daughter cells

also displayed strong migration and invasion abilities [6]. However, the mechanism of PGCCs with daughter cells promoting tumor metastasis, invasion, and proliferation remains unclear.

Our previous study has confirmed that S100A10 was significantly upregulated in PGCCs with daughter cells after $CoCl_2$ treatment compared with the control cells [7]. S100A10 is a member of the S100 family of EF-hand-type Ca^{2+}-binding proteins [8, 9]. S100A10 usually associates with annexin A2 (ANXA2) to form a heterotetramer complex (AIIt) and is mainly localized to the cell membrane and cytoplasm. AIIt in the cytoplasm can protect S100A10 from ubiquitin-mediated proteasome degradation [10]. S100A10 in the cell membrane and cytoplasm plays an important role in the infiltration and invasion of malignant tumors. However, the mechanism of S100A10 nuclear localization in malignant tumors has not been reported.

In this study, we confirmed that S100A10 was localized to the nucleus in PGCCs and their daughter cells. The nuclear translocation of S100A10 in PGCCs and their daughter cells was regulated by SUMOylation, and the SUMOylated S100A10 regulated the mRNA expression of *DEFA3*, *PTPRN2* and *ARHGEF18*, which promoted tumor proliferation, metastasis, and invasion.

Materials And Methods

Cell lines and induction of PGCCs formation after $CoCl_2$ treatment

Hct116 and LoVo CRC cells were obtained from the American Type Culture Collection and grown in complete RPMI-1640. The detailed information about $CoCl_2$ treatment was described in Supplementary Materials and Methods.

Western blots (WB) analysis

$CoCl_2$ treated and untreated cells were collected. Total, cytoplasmic, and nuclear proteins were extracted according to the manufacturer's instructions (Thermo Fisher Scientific; #SJ252790). The detailed information is provided in the supplementary table 1 and supplementary materials and methods.

Cell migration and invasion assays

The abilities of cell migration and invasion assay were evaluated as previously described [11] and detailed information about these assays were provided in the Supplementary Materials and Methods.

Colony formation assay

The detailed information is provided in the Supplementary Materials and Methods.

Immunocytochemical and immunohistochemical staining

The detailed information is provided in the supplementary table 1 and supplementary materials and methods.

Co-immunoprecipitation

Co-IP was used to determine the interactions of SUMO1-S100A10 and ubiquitin-S100A10 in LoVo and Hct116 cells before and after $CoCl_2$ treatment. The detailed information is provided in the Supplementary Materials and Methods.

Cell viability assay

The cell viability assay after Ginkgolic acid (GA,15:1) treatment is provided in Supplementary Materials and Methods.

Ginkgolic acid (15:1) and MG132 treatment

MG132 is a proteasome inhibitor that can impair ubiquitin-mediated proteasome degradation. The cells before and after the treatment of $CoCl_2$ were grown in 6-well plates until they reached 80% confluence. MG132 (10 μM, Selleck Chemicals, USA) was added, and cell samples were collected for later experiments after incubation for 6 h. Different concentrations (5, 10, and 20 μM) of GA (15:1, MedChem Express, USA) were added to the control cells and PGCCs with daughter cells for 24 h, followed by western blot analysis and other assays.

5-fluorouracil and Oxaliplatin treatment

LoVo and Hct116 cells were treated by 5-Fu and Oxa as previously described [6]. The detailed information is provided in the Supplementary Materials and Methods.

Transient siRNA transfection

The detailed information about transient siRNA transfection is provided in the supplementary table 2, 3 and supplementary materials and methods.

Chromatin immunoprecipitation and data analysis

ChIP assays were performed according to the instructions of the Pierce Magnetic ChIP Kit. MEME [12] and DREME [13] were used to detect the sequence motif, which was used to detect long and short consensus sequences. The position of peak summit around the transcript start sites of genes can predict the interaction sites of proteins and genes. Genes associated with different peaks were identified, and GO and KEGG enrichment analyses were performed. The detailed information is provided in the Supplementary Materials and Methods.

Real-time PCR analysis

The detailed information is provided in the Supplementary Materials and Methods. The sequences of PCR primers are shown in supplemental table 4.

Human CRC samples

Paraffin-embedded human CRC tissue samples (n=218) were obtained from the Department of Pathology of Tianjin Union Medical Center. These tissues were divided into four groups: 55 cases of well-differentiated primary focus (group I), 53 cases of moderately differentiated primary focus (group II), 52 cases of poorly differentiated primary focus (group III), and 58 cases of lymph node metastatic foci (group IV). This study was approved by the Hospital Review Board of Tianjin Union Medical Center, and patient information confidentiality was maintained.

Scoring of IHC Staining

Protein expression was evaluated as previously described [11]. The detailed information is provided in the Supplementary Materials and Methods.

Statistical analyses

SPSS 22 (SPSS Inc., Chicago, USA) was used to analyze the data in this study. All column diagram data are expressed as means±SD, and all table data are presented as means±SEM. The Kruskal-Wallis test was conducted to compare the differences in S100A10-related protein expression in human CRC tissues. Other comparisons were performed using a two-tailed Student's *t*-test and Pearson chi-square (χ^2) test. A two-tailed *P* value <0.05 was considered statistically significant.

Results

Formation of PGCCs induced by CoCl2 treatment

LoVo and Hct116 cells were cultured in T25 flasks to reach 70-80% confluence and treated with 450 μM of $CoCl_2$ for 48-72 h (Fig. 1A -a, -c). After treatment, most of the small-sized tumor cells died, whereas a few scattered PGCCs survived. The size of PGCCs was significantly larger than that of the control cells (Fig. 1A -b, -d). Approximately 10-15 days later, the surviving PGCCs had recovered from $CoCl_2$ treatment and generated small-sized daughter cells via asymmetric division. After repeating this treatment 3-4 times, 20-30% of PGCCs and 70-80% of their daughter cells were observed in the flask. The properties of PGCCs and their daughter cells have been well documented in our previous studies [1, 4, 5, 7].

Daughter cells derived from PGCCs have strong abilities of migration, invasion, and proliferation

The results of the transwell assay showed that PGCCs with daughter cells gained higher migratory and invasive capacities in comparison with those in the control cells (Fig. S1A, S1B). Additionally, the wound-healing assay showed that the migration ability of LoVo and Hct116 PGCCs with daughter cells was significantly increased compared with that of the control cells (Fig. S1D, S1E). A plate colony formation

assay demonstrated that the proliferation ability in PGCCs with daughter cells was higher than that in the control cells (Fig. S1G, S1H).

S100A10 is expressed in both the cytoplasm and nuclei of PGCCs with daughter cells

S100A10 was previously reported to be localized in the cytoplasm or membrane. In this study, the expression of S100A10 and ANXA2 was higher in PGCCs and their daughter cells than in the control cells (Fig. 1B, 1C). In the control cells, S100A10 was detected only in the cytoplasm. In PGCCs and their daughter cells, S100A10 was detected in both the cytoplasm (Fig. 1B, 1C) and nucleus (Fig. 1F). ANXA2 was only detected in the cytoplasm (Fig. 1B, 1C, 1F). The nuclear localization of S100A10 in the PGCCs and their daughter cells was also confirmed using immunocytochemical (ICC) staining (Fig. 1G, 1H). In addition, S100A10 in PGCCs and their daughter cells was knocked down by transient transfection of S100A10-siRNA sequences (740, 682, 514). The inhibition efficiency was evaluated using western blotting (Fig. 1I, 1J). The migration, invasion, and proliferation abilities of PGCCs and their daughter cells were compared before and after S100A10-740i treatment. Figure S2A and S2B show that the migration and invasion abilities of cells after S100A10 knockdown (S100A10i) treatment were lower than those in the negative control (NC). The results of the wound-healing assay indicated that the migration ability decreased after S100A10i treatment (Fig. S2C, S2D). Plate cloning assay confirmed that there were less clones formed in LoVo and Hct116 PGCCs and their daughter cells after S100A10i than in 30, 60, and 120 NC cells (Fig. S2 G, S2H). S100A10 knockdown resulted in significant decrease in invasion, migration, and proliferation abilities of PGCCs and their daughter cells (Fig. S2E, S2I).

S100A10 is modified by SUMOylation in PGCCs and their daughter cells

S100A10 can be modified by ubiquitination and thus degraded by the proteasome, which can be inhibited by ANXA2 [14]. Co-immunoprecipitation was used to detect the interaction between ubiquitin, SUMO1, and S100A10. The total cell lysates of the control and PGCCs with daughter cells were immunoprecipitated with an anti-S100A10 antibody (Fig. 2A, 2B), and then immunoblotted with anti-ubiquitin (linkage-specific K48) and anti-SUMO1 antibodies, respectively. There was not interaction between S100A10 and ubiquitin in PGCCs with their daughter cells (Fig. 2E, 2F). MG132 is a proteasome inhibitor that protects ubiquitinated proteins from proteasome-mediated degradation. After treatment with MG132, the expression of S100A10 was detected in both the control cells and PGCCs with daughter cells (Fig. 2G, 2H). In the control cells, the expression level of S100A10 was significantly increased (Fig. 2L -a). However, there was no significant difference in the expression of S100A10 in PGCCs with daughter cells before and after MG132 treatment (Fig. 2L -b). These results indicated that S100A10 might not be ubiquitinated in PGCCs and their daughter cells.

In the PGCCs with daughter cells, the interaction between SUMO1 and S100A10 was stronger than in the control cells (Fig. 2C, 2D). GA could inhibit SUMOylation *in vitro* and was used to treat the control cells and PGCCs with daughter cells. After GA treatment, the expression level of S100A10 was significantly decreased in PGCCs with daughter cells compared to the control cells, which could be eliminated by both MG132 and GA treatment (Fig. 2I, 2J). There was no change in the expression of S100A10, ANXA2, and

ANXA2-P-Y23 in the control cells before and after GA treatment (Fig. 3H, 3I). The results showed that S100A10 was mainly modified by ubiquitin in the control cells, while it was modified by SUMOylation in the PGCCs with daughter cells.

GA reduced the nuclear expression of S100A10 and inhibited the migration, invasion, and proliferation of PGCCs with daughter cells

To determine whether SUMOylation contributed to the nuclear localization of S100A10, GA was used to treat PGCCs with daughter cells. The cell counting kit-8 (CCK8) assay was performed in PGCCs with daughter cells to determine the appropriate concentration and incubation time (Fig. 3A). Our results demonstrated that GA inhibited the proliferation of PGCCs with daughter cells in a time- and dose-dependent manner. Cell viability was seriously impaired at 40 μM for 24 h, and GA at concentrations of 5, 10, and 20 μM was used in this study.

After incubating with different GA concentrations for 24 h, the cells were collected. The total, cytosolic, and nuclear fractions were collected to detect the expression of S100A10, ANXA2, and ANXA2-P-Y23. In the total and cytosolic fractions, the expression of S100A10 and ANXA2 gradually decreased as the increasing concentration of GA treatment (Fig. 3B, 3C; Fig. S2F -a, -b, -d, -e; Fig. S3G -a, -b, -d, -e). The expression of ANXA2-P-Y23 was mildly changed (Fig. 3B, 3C), and the phosphorylated level of ANXA2 was significantly increased (Fig. S2F -c, -f; Fig. S3G -c,–f) in the total and cytosolic fractions. The nuclear localization of S100A10 was inhibited by GA treatment in a dose-dependent manner, indicating that SUMOylation might play an important role in the nuclear localization of S100A10 (Fig. 3F, 3G; Fig. S2 F -g; Fig. S3G -g).

To assess the effect of GA on the migration, invasion, and proliferation of PGCCs with daughter cells, cells before and after treatment with 20μM GA were used. The results of the wound-healing assay showed that the scratched areas of the PGCCs with daughter cells before GA treatment were significantly narrower than those in the cells after GA treatment (Fig. S3C, S3D). The results of the transwell assay showed that the number of migratory and invasive cells among the PGCCs with daughter cells treated with GA was lower than that in the untreated cells (Fig. S3A, S3B). The number of colonies of 30, 60, and 120 GA-treated PGCCs with daughter cells was reduced compared with that in the untreated cells (Fig. S3E, S3F).

SUMO1 knockdown inhibits the nuclear localization of S100A10 and decreases the migration, invasion, and proliferation abilities of PGCCs and their daughter cells

To further confirm the effects of SUMOylation on the nuclear localization of S100A10, we performed transient transfection by using SUMO1-siRNA sequences (307, 358, 727) to knockdown the expression of SUMO1 in PGCCs with their daughter cells. After transfection, cell samples were immunoblotted with an ani-SUMO1 antibody to detect the transfection effects (Fig. 4A, 4B). The total and cytoplasmic expression of S100A10 was declined after SUMO1 knockdown (Fig. 4C-F). The nuclear localization of S100A10 was completely inhibited by SUMO1-siRNA transfection in PGCCs with daughter cells (Fig. 4G, 4H). Total and

cytoplasmic levels of ANXA2 were moderately downregulated after SUMO1 knockdown, which was also statistically significant (Fig. 4C-F). The level of phosphorylated ANXA2 at tyrosine 23 did not change and the total ANXA2 level decreased after SUMO1 knockdown (Fig. 4C, 4D, and 4J -c, -d, 4K -c, -d).

Inhibition of SUMO1 expression also decreased the migration, invasion, and proliferation of PGCCs with daughter cells. In the wound-healing assay, the wound spaces in the NC group were smaller than those of the SUMO1 knockdown (**Fig. 5A, 5B, 5G- a**). The results of the transwell assay further demonstrated that the migration and invasion abilities were decreased after SUMO1 knockdown **(Fig. 5C, 5D, 5G- b, 5H -a**). The colony formation efficiency after SUMO1 knockdown was significantly lower than that in the NC group (**Fig. 5E, 5F, 5H-b**).

ICC staining of S100A10 further demonstrated that SUMOylation was involved in the nuclear localization of S100A10. In PGCCs with daughter cells, the expression of S100A10 was observed in both the cytoplasm and nucleus (Fig. 5I -a, -d). When PGCCs with daughter cells were treated with 20 μM of GA or transfected with SUMO1 siRNA, the expression of S100A10 was only observed in the cytoplasm (Fig. 5I -b, -c, -e, -f).

The nuclear localization of S100A10 regulates the expression of *DEFA3*, *PTPRN2,* and *ARGHEF18*

Chromatin immunoprecipitation (ChIP) assay was performed using an antibody against S100A10, followed by sequencing to assess the potential targets of S100A10. The results showed that 4148 significant ChIP-seq peaked in Hct116-derived PGCCs with daughter cells, and 1380 peaked in LoVo-derived PGCCs with daughter cells. Genes with overlapping peaks were then enriched by Gene Ontology [GO] (Fig. 5J, -a, -b). Moreover, Kyoto Encyclopedia of Genes and Genomes (KEGG) pathway analysis revealed the potential targets (Fig. 5J, -c, -d). According to the gene function, *DEFA3*, *PTPRN2*, and *ARHGEF18* were selected, which are associated with the regulation of cytoskeleton dynamics and cell migration. DNA samples for the ChIP assay isolated from the PGCCs wand their daughter cells before and after SUMO1 knockdown were analyzed using real-time PCR. The results showed that all the levels of immunoprecipitated DNA of *DEFA3*, *PTPRN2,* and *ARHGEF18* bound to S100A10 were decreased after SUMO1 knockdown (Fig. 5K). The protein levels of ARHGEF18, DEFA3, and PTPRN2 were upregulated in PGCCs with daughter cells (Fig. 5L; Fig S4 A).

The total protein expression levels of ARHGEF18, DEFA3, and PTPRN2 were decreased after S100A10i treatment (Fig. 6A; Fig. S3 H, I). To further study the effect of SUMOylated S100A10 on the expression of ARHGEF18, DEFA3, and PTPRN2, PGCCs with daughter cells were treated with 0, 5, 10, and 20 μM of GA and the total expression levels of ARHGEF18, DEFA3, and PTPRN2 were gradually decreased in a concentration-dependent manner (Fig. 6B; Fig S2. F -h, -I, -j; Fig S3 G -h, -i, -j). The total expression of ARHGEF18, DEFA3, and PTPRN2 was also decreased when S100A10 expression was decreased after SUMO1 knockdown (Fig. 6C; Fig. S4B).

5-fluorouracil (5-Fu) and oxaliplatin (Oxa) treatment promotes the nuclear localization of S100A10 by SUMOylation

To study the effect of chemotherapeutic drug treatment on the expression and subcellular localization of S100A10 in CRC cells, LoVo and Hct116 were treated with 5-Fu and Oxa for three times. The nuclear expression level of S100A10 increased after 5-Fu and Oxa treatment (Fig. 6D; Fig S4C -c). The total and cytoplasmic expression of ANXA2 and S100A10 was increased after treatment with 5-Fu and Oxa (Fig. 6E, 6F; Fig S4C -a, -b, -d, -e). The total cell lysates of the 5-Fu- and Oxa-treated cells were immunoprecipitated with an anti-S100A10 antibody (Fig. 6G, 6H) and immunoblotted with an anti-SUMO1 antibody (Fig. 6I, 6J). The results showed that S100A10 was modified by SUMOylation after 5-Fu and Oxa treatment. The expression levels of ARHGEF18, DEFA3 and PTPRN2 were upregulated after 5-Fu and Oxa treatment (Fig. 6F; Fig S4E).

Expression of S100A10-related protein in human CRC tissues

Human CRC tissues were used to evaluate the association between S100A10 expression level, tumor differentiation, and lymph node metastatic foci (Fig. 6K, a, b, c). The differences in S100A10 staining index among the four groups were statistically significant (P=0.000, table-1). In addition, the expression of S100A10 was mainly distributed in the cytoplasm of tumor cells in group I (Fig. 6K, d). In group III, S100A10 expression was located in both the cytoplasm and nucleus of cancer cells (Fig. 6K, e). The staining index of S100A10 nuclear expression was significantly higher in poorly differentiated CRC than in well-differentiated CRC (P=0.000) and moderately differentiated CRC (P=0.018). The staining index of S100A10 nuclear expression was also higher in lymph node metastatic foci than in well-differentiated CRC (P=0.000) and moderately differentiated CRC (P=0.003) (table 2). S100A10 was localized in both the cytoplasm and nucleus of PGCCs (Fig. 6K -f).

Discussion

$CoCl_2$ and chemoradiotherapy can induce the formation of PGCCs, and daughter cells derived from these PGCCs have strong abilities of proliferation, infiltration, and invasion. Studies have demonstrated that PGCCs with daughter cells could exert important influences on the progression of malignant tumors, including metastasis, chemoresistance, and tumor relapse [15–23]. Here, we demonstrated that S100A10 was involved in regulating the migration and invasion of PGCCs with daughter cells in CRC cells.

The membrane-localized S100A10 promotes cancer invasion by regulating tissue plasminogen activator activity and plasmin generation [24]. S100A10 is unable to exist in the absence of ANXA2 and is promptly degraded when cytoplasmic ANXA2 is depleted [10, 25]. S100A10 is an ubiquitin-modified protein that can be degraded by proteasomes. Lu et al. reported that S100A10 and ANXA2 were both observed in the nucleus of breast cancer stem cells after paclitaxel treatment [26]. However, the mechanism by which S100A10 and ANXA2 are transported into the nucleus has not been reported. Under hypoxic conditions, the levels of SUMOylated proteins increase in cancer cells, including those modified with SUMO-1 [27]. SUMOylation is a prevalent post-translation modification that occurs at the lysine residue and can regulate the response of cells to stress [28]. In this study, $CoCl_2$ was used to induce the formation of PGCCs and their daughter cells. The expression levels of S100A10 and ANXA2 were increased in the total

and cytoplasmic fractions after $CoCl_2$ treatment. S100A10 and ANXA2 were mainly expressed in the cytoplasm of control cells. However, the results of WB and ICC showed that S100A10 was also detected in the nuclear fractions of PGCCs and their daughter cells, while ANXA2 was not detected in the nucleus.

Results of S100A10 Co-immunoprecipitation showed that ubiquitin-modified S100A10 was expressed in the control cells, and SUMO1-modified S100A10 appeared in the PGCCs with daughter cells, which confirmed that S100A10 was mainly modified by SUMOylation after $CoCl_2$ treatment. This result was further confirmed by the treatment with MG132 and GA. The expression of S100A10 increased in the control cells, and there was no change in S100A10 expression in the PGCCs with daughter cells after MG132 treatment. After GA treatment, the nuclear expression of S100A10 was gradually decreased, which indicated that SUMOylation directly mediated the nuclear localization of S100A10. Furthermore, the total and cytoplasmic expression of S100A10 was also decreased in PGCCs with daughter cells after GA treatment, which showed that S100A10 was re-ubiquitinated because the lysine site became accessible after SUMOylation was inhibited. To determine the re-ubiquitin of S100A10, the PGCCs with daughter cells were treated with both MG132 and GA. Compared with the cells treated with GA alone, the decrease in S100A10 increased again after proteasome inhibition. Furthermore, the formation of AIIt in the cytoplasm can protect S100A10 from ubiquitin-dependent proteasome degradation, and the phosphorylation of tyrosine 23 can promote the formation of the complex. The expression of ANXA2 was also decreased after GA treatment. The nuclear expression of S100A10 was blocked in PGCCs with daughter cells as well as in the cytoplasm after SUMO1 knockdown. GA treatment and SUMO1 knockdown inhibited the migration, invasion, and proliferation of PGCCs with daughter cells. MG132 can inhibit ubiquitin-mediated proteasome degradation, and the expression level of S100A10 should be increased after MG132 treatment. SUMOylation can stabilize the expression of S100A10 by competing with ubiquitination and facilitating the nuclear localization of S100A10. The results showed that the inhibition of S100A10 SUMOylation could impair the migration, invasion, and proliferation of PGCCs with daughter cells. Based on these results, we can conclude that S100A10 was modified by SUMOylation in PGCCs with daughter cells and by ubiquitination in control cells. The nuclear localization of S100A10 is regulated by SUMOylation.

Furthermore, results of the ChIP-Seq assay indicated that S100A10 modulated the expression of *ARHGEF18*, *PTPRN2*, and *DEFA3* in PGCCs with daughter cells. ARHGEF18, PTPRN2, and DEFA3 associated with actin dynamics and cytoskeleton remodeling [29, 30]. Results of the real-time PCR confirmed that the DNA levels of *ARHGEF18*, *PTPRN2*, and *DEFA3* bound to S100A10 were decreased after SUMO1 knockdown in the PGCCs with daughter cells. The downregulation of ARHGEF18, PTPRN2, and DEFA3 in the PGCCs with daughter cells after S100A10 knockdown indicated that S100A10 served as an upstream factor of these three proteins. Inhibition of SUMOylation in PGCCs with daughter cells either by GA treatment or SUMO1 silencing could also inhibit the expression of ARHGEF18, PTPRN2, and DEFA3, which further confirmed that the expression of these proteins can be inhibited after SUMOylated S100A10 inhibition. S100A10 expression increased in both the cytoplasm and nucleus, and S100A10 was modified by SUMOylation in PGCCs with daughter cells induced by 5-Fu and Oxa treatment. The

expression levels of ARHGEF18, PTPRN2, and DEFA3 were also increased. In human CRC tissues, the expression level of S100A10 was positively correlated with tumor differentiation.

Conclusion

S100A10 can be modified by SUMOylation in PGCCs and their daughter cells induced by $CoCl_2$ and chemoradiotherapy. SUMO1-modified S100A10 can translocate to the nucleus and regulate the expression of ARHGEF18, PTPRN2, and DEFA3 to promote the proliferation, migration, and invasion of PGCCs and their daughter cells.

Abbreviations

PGCCs: polyploid giant cells; $CoCl_2$: cobalt chloride; iTRAQ: isobaric tags for relative and absolute quantification; GA: ginkgolic acid; WB: Western blotting; 5-Fu: 5-fluorouracil; Oxa: oxaliplatin; SUMO: small ubiquitin-like modifier; CRC: colorectal cancer; DEFA3: **neutrophil defensin 3;** PTPRN2: receptor-type tyrosine-protein phosphatase N2; ARHGEF18: rho guanine nucleotide exchange factor 18; MMP: matrix metalloproteinase; NC: negative-control; A□t: a hereotetramer combined with S100A10 and ANXA2; LARC: locally advanced rectal cancer; CRC: colorectal cancer; ANXA2: Annexin A2; t-PA: tissue plasminogen activator; ICC: immunocytochemical; IHC: immunohistochemical; co-IP: co-immunoprecipitation; ChIP: Chromatin immunoprecipitation; GO: gene ontology; KEGG: Kyoto Encyclopedia of Genes and Genomes.

Declarations

Acknowledgements

We would like to thank Editage (www.editage.cn) for English language editing.

Authors' contributions

SZ designed the study and interpreted data; contributed to manuscript writing; and approved the manuscript before submission. QZ, KZ and ZL collected and analyzed data and approved the manuscript before submission. ZL, HZ and FF collected, analyzed, and interpreted data, and approved the manuscript before submission. MZ, collected data, gave constructive comments on the manuscript, and approved the manuscript before submission.

Fundings

This work was supported in part by grants from the National Natural Science Foundation of China (81672426), and Foundation of the committee on science and technology of Tianjin (17ZXMFSY00120).

Availability of data and materials

The authors declare that all data supporting the findings of this study are available within the article and its additional files or contact the corresponding author upon reasonable request.

Ethics approval and consent to participate

The use of human tissue samples was approved by the Hospital Review Board and the confidentiality of patient information was maintained.

Consent for publication

All authors have agreed to publish this manuscript.

Competing interests

The authors declare that they have no competing interests.

Authors' information

[1]Department of Pathology, Tianjin Union Medical Center, Tianjin, P.R. China. [2]Nankai University School of Medicine, Nankai University, Tianjin, P.R.China.

[3]Graduate School, Tianjin University of Traditional Chinese Medicine, Tianjin, P.R. China.

References

1. Zhang S, Mercado-Uribe I, Xing Z, Sun B, Kuang J, Liu J: **Generation of cancer stem-like cells through the formation of polyploid giant cancer cells**. *Oncogene* 2014, **33**(1):116-128.
2. Fei F, Li C, Wang X, Du J, Liu K, Li B, Yao P, Li Y, Zhang S: **Syncytin 1, CD9, and CD47 regulating cell fusion to form PGCCs associated with cAMP/PKA and JNK signaling pathway**. *Cancer medicine* 2019, **8**(6):3047-3058.
3. Fei F, Liu K, Li C, Du J, Wei Z, Li B, Li Y, Zhang Y, Zhang S: **Molecular Mechanisms by Which S100A4 Regulates the Migration and Invasion of PGCCs With Their Daughter Cells in Human Colorectal Cancer**. *Frontiers in oncology* 2020, **10**:182.
4. Fei F, Qu J, Liu K, Li C, Wang X, Li Y, Zhang S: **The subcellular location of cyclin B1 and CDC25 associated with the formation of polyploid giant cancer cells and their clinicopathological significance**. *Laboratory investigation; a journal of technical methods and pathology* 2019, **99**(4):483-498.
5. Fei F, Zhang D, Yang Z, Wang S, Wang X, Wu Z, Wu Q, Zhang S: **The number of polyploid giant cancer cells and epithelial-mesenchymal transition-related proteins are associated with invasion and metastasis in human breast cancer**. *Journal of experimental & clinical cancer research : CR* 2015, **34**:158.

6. Fei F, Zhang M, Li B, Zhao L, Wang H, Liu L, Li Y, Ding P, Gu Y, Zhang X *et al*: **Formation of Polyploid Giant Cancer Cells Involves in the Prognostic Value of Neoadjuvant Chemoradiation in Locally Advanced Rectal Cancer**. *Journal of oncology* 2019, **2019**:2316436.
7. Zhang S, Mercado-Uribe I, Hanash S, Liu J: **iTRAQ-based proteomic analysis of polyploid giant cancer cells and budding progeny cells reveals several distinct pathways for ovarian cancer development**. *PloS one* 2013, **8**(11):e80120.
8. Hermann A, Donato R, Weiger TM, Chazin WJ: **S100 calcium binding proteins and ion channels**. *Front Pharmacol* 2012, **3**:67.
9. Donato R, Cannon BR, Sorci G, Riuzzi F, Hsu K, Weber DJ, Geczy CL: **Functions of S100 proteins**. *Current molecular medicine* 2013, **13**(1):24-57.
10. He KL, Deora AB, Xiong H, Ling Q, Weksler BB, Niesvizky R, Hajjar KA: **Endothelial cell annexin A2 regulates polyubiquitination and degradation of its binding partner S100A10/p11**. *The Journal of biological chemistry* 2008, **283**(28):19192-19200.
11. Liu K, Zheng M, Zhao Q, Zhang K, Li Z, Fu F, Zhang H, Du J, Li Y, Zhang S: **Different p53 genotypes regulating different phosphorylation sites and subcellular location of CDC25C associated with the formation of polyploid giant cancer cells**. *Journal of experimental & clinical cancer research : CR* 2020, **39**(1):83.
12. Bailey TL, Elkan C: **Fitting a mixture model by expectation maximization to discover motifs in biopolymers**. *Proc Int Conf Intell Syst Mol Biol* 1994, **2**:28-36.
13. Bailey TL: **DREME: motif discovery in transcription factor ChIP-seq data**. *Bioinformatics* 2011, **27**(12):1653-1659.
14. Li C, Ma Y, Fei F, Zheng M, Li Z, Zhao Q, Du J, Liu K, Lu R, Zhang S: **Critical role and its underlying molecular events of the plasminogen receptor, S100A10 in malignant tumor and non-tumor diseases**. *Journal of Cancer* 2020, **11**(4):826-836.
15. Lv H, Shi Y, Zhang L, Zhang D, Liu G, Yang Z, Li Y, Fei F, Zhang S: **Polyploid giant cancer cells with budding and the expression of cyclin E, S-phase kinase-associated protein 2, stathmin associated with the grading and metastasis in serous ovarian tumor**. *BMC cancer* 2014, **14**:576.
16. Xuan B, Ghosh D, Cheney EM, Clifton EM, Dawson MR: **Dysregulation in Actin Cytoskeletal Organization Drives Increased Stiffness and Migratory Persistence in Polyploidal Giant Cancer Cells**. *Scientific reports* 2018, **8**(1):11935.
17. Chen J, Niu N, Zhang J, Qi L, Shen W, Donkena KV, Feng Z, Liu J: **Polyploid Giant Cancer Cells (PGCCs): The Evil Roots of Cancer**. *Current cancer drug targets* 2019, **19**(5):360-367.
18. Wang Q, Lu F, Lan R: **RNA-sequencing dissects the transcriptome of polyploid cancer cells that are resistant to combined treatments of cisplatin with paclitaxel and docetaxel**. *Molecular bioSystems* 2017, **13**(10):2125-2134.
19. Niu N, Mercado-Uribe I, Liu J: **Dedifferentiation into blastomere-like cancer stem cells via formation of polyploid giant cancer cells**. *Oncogene* 2017, **36**(34):4887-4900.

20. Mirzayans R, Andrais B, Murray D: **Roles of Polyploid/Multinucleated Giant Cancer Cells in Metastasis and Disease Relapse Following Anticancer Treatment**. *Cancers* 2018, **10**(4).
21. Arun RP, Sivanesan D, Patra B, Varadaraj S, Verma RS: **Simulated microgravity increases polyploid giant cancer cells and nuclear localization of YAP**. *Scientific reports* 2019, **9**(1):10684.
22. Bharadwaj D, Mandal M: **Senescence in polyploid giant cancer cells: A road that leads to chemoresistance**. *Cytokine & growth factor reviews* 2020, **52**:68-75.
23. Wang X, Zheng M, Fei F, Li C, Du J, Liu K, Li Y, Zhang S: **EMT-related protein expression in polyploid giant cancer cells and their daughter cells with different passages after triptolide treatment**. *Medical oncology* 2019, **36**(9):82.
24. Bresnick AR, Weber DJ, Zimmer DB: **S100 proteins in cancer**. *Nat Rev Cancer* 2015, **15**(2):96-109.
25. Puisieux A, Ji J, Ozturk M: **Annexin II up-regulates cellular levels of p11 protein by a post-translational mechanisms**. *Biochem J* 1996, **313 (Pt 1)**:51-55.
26. Lu H, Xie Y, Tran L, Lan J, Yang Y, Murugan NL, Wang R, Wang YJ, Semenza GL: **Chemotherapy-induced S100A10 recruits KDM6A to facilitate OCT4-mediated breast cancer stemness**. *J Clin Invest* 2020, **130**(9):4607-4623.
27. Shao R, Zhang FP, Tian F, Anders Friberg P, Wang X, Sjoland H, Billig H: **Increase of SUMO-1 expression in response to hypoxia: direct interaction with HIF-1alpha in adult mouse brain and heart in vivo**. *FEBS letters* 2004, **569**(1-3):293-300.
28. Guo C, Henley JM: **Wrestling with stress: roles of protein SUMOylation and deSUMOylation in cell stress response**. *IUBMB life* 2014, **66**(2):71-77.
29. Nagata K, Inagaki M: **Cytoskeletal modification of Rho guanine nucleotide exchange factor activity: identification of a Rho guanine nucleotide exchange factor as a binding partner for Sept9b, a mammalian septin**. *Oncogene* 2005, **24**(1):65-76.
30. Gunes M, Gecit I, Pirincci N, Kemik AS, Purisa S, Ceylan K, Aslan M: **Plasma human neutrophil proteins-1, -2, and -3 levels in patients with bladder cancer**. *Journal of cancer research and clinical oncology* 2013, **139**(2):195-199.

Tables

Table 1. Differences of S100A10 staining index in different group of human CRCs.

	group	n	Staining index for S100A10	Value of statistics	*P*
Well-differentiated CRCs	group	55	2.800±1.967	χ^2= 51.973	0.000*
Moderately differentiated CRCs	group	53	3.641±2.207		
Poorly differentiated CRCs	group	52	6.442±1.895		
Lymph node metastatic foci	group	58	5.645±2.076		

**P*<0.05: statistically significant. (*P*: difference among the three groups; *P*1 (difference between groups I and II)=0.002; *P*2 (difference between groups and)=0.000; *P*3 (difference between groups and)=0.593; *P*4 (difference between groups I and IV)<0.000; *P*5 (difference between groups II and IV) =0.000. CRCs: colorectal cancers.

Table 2. Comparison of staining index of S100A10 nuclear expression in human CRC tissues.

	group	n	Staining index for S100A10	Value of statistics	*P*
Well-differentiated CRCs	group	55	1.000±0.000	χ^2=44.108	0.000*
Moderately differentiated CRCs	group	53	1.377±0.713		
Poorly differentiated CRCs	group	52	1.712±0.824		
Lymph node metastatic foci	group	58	1.827±0.861		

**P*<0.05: statistically significant. (*P*: difference among the four groups; *P*1 (difference between groups I and II)=0.000; *P*2 (difference between groups and)=0.018; *P*3 (difference between groups and)=0.485; *P*4 (difference between groups I and IV)=0.000; *P*5 (difference between groups II and IV)=0.003. CRC: colorectal cancer.

Figures

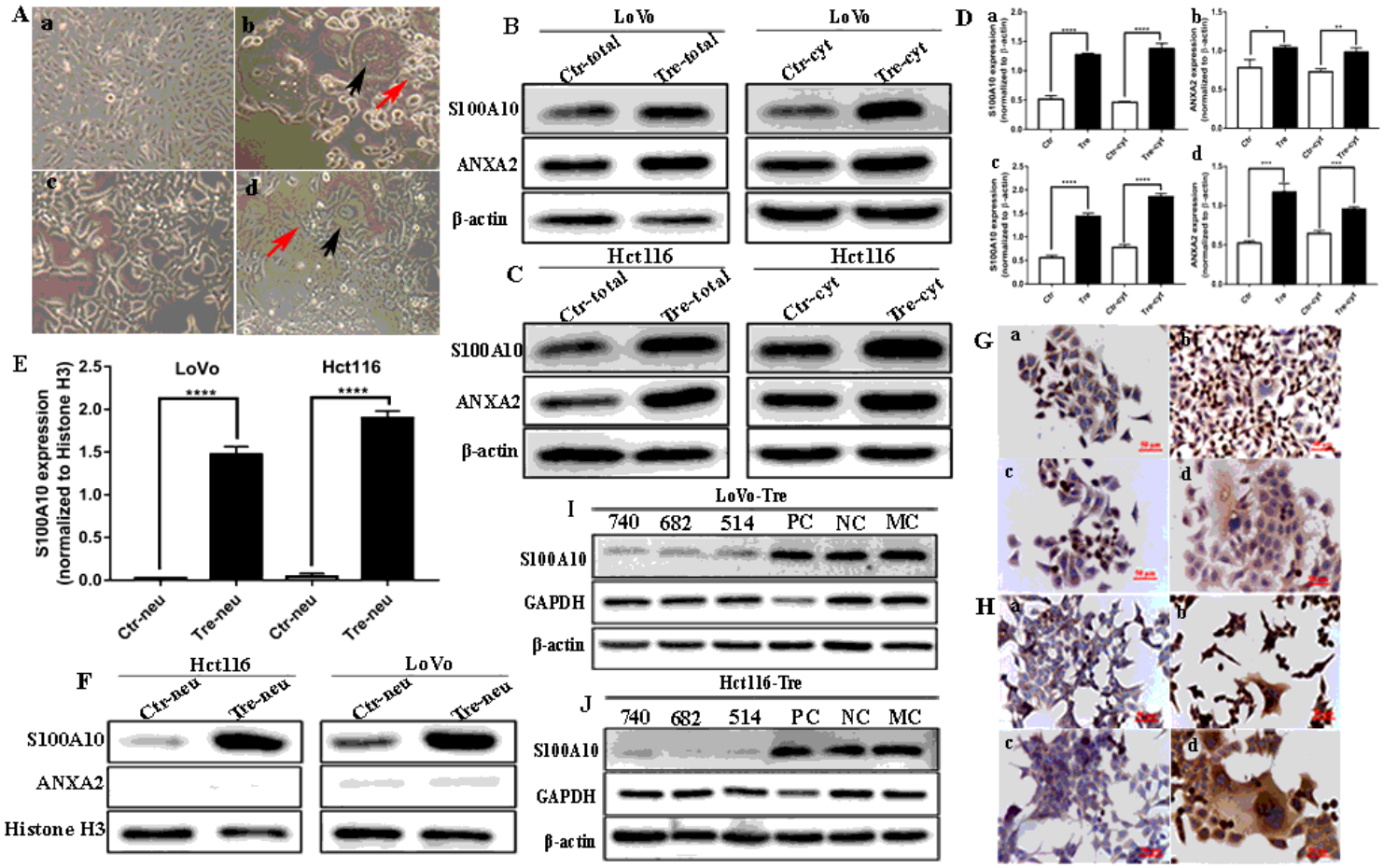

Figure 1

S100A10 and ANXA2 expression in Lovo and Hct116 cells before and after CoCl2 treatment. A. Control cells and PGCCs with daughter cells derived from LoVo and Hct116 (100×). (a) LoVo control cells. (b) LoVo PGCCs and daughter cells. Black arrow indicates PGCC. Red arrow indicates daughter cells. (c) Hct116 control cells. (d) Hct116 PGCCs with daughter cells. Black arrow indicates PGCC. Red arrow indicates daughter cells. B. The total and cytoplasmic S100A10 and ANXA2 expression in LoVo cells before and after CoCl2 treatment. C. The total and cytoplasmic S100A10 and ANXA2 expression in Hct116 cells before and after CoCl2 treatment. D. (a) Comparison of the total and cytoplasmic S100A10 expression in LoVo cells before and after CoCl2 treatment. (b) Comparison of the total and cytoplasmic expression of ANXA2 in LoVo cells before and after CoCl2 treatment. (c) Comparison of the total and cytoplasmic S100A10 expression in Hct116 cells before and after CoCl2 treatment. (d) Comparison of the total and cytoplasmic ANXA2 expression in Hct116 cells before and after CoCl2 treatment. E. Comparison of the nuclear S100A10 expression in Hct116 and LoVo cells before and after CoCl2 treatment. F. The nuclear S100A10 and ANXA2 expression in Hct116 and LoVo cells before and after CoCl2 treatment. G. ICC staining for S100A10 and ANXA2 in LoVo cells before and after CoCl2 treatment (ICC, 400×). (a)

S100A10 in LoVo control cells (b) S100A10 in LoVo PGCCs with their daughter cells. (c) ANXA2 in LoVo control cells. (d) ANXA2 in LoVo PGCCs with their daughter cells. H. ICC staining of S100A10 and ANXA2 in Hct116 cells before and after CoCl2 treatment (ICC, 400×). (a) S100A10 in Hct116 control cells (b) S100A10 in Hct116 PGCCs with their daughter cells. (c) ANXA2 in Hct116 control cells. (d) ANXA2 in Hct116 PGCCs with their daughter cells. I. Total S100A10 expression in LoVo PGCCs with their daughter cells after siRNA S100A10-740, 682, 514, siRNA control and negative control transfection. J. Total S100A10 expression in Hct116 PGCCs with daughter cells after siRNA S100A10-740, 682, 514, siRNA control and negative control transfection. Ctr: control cells; Tre: cells treated with CoCl2

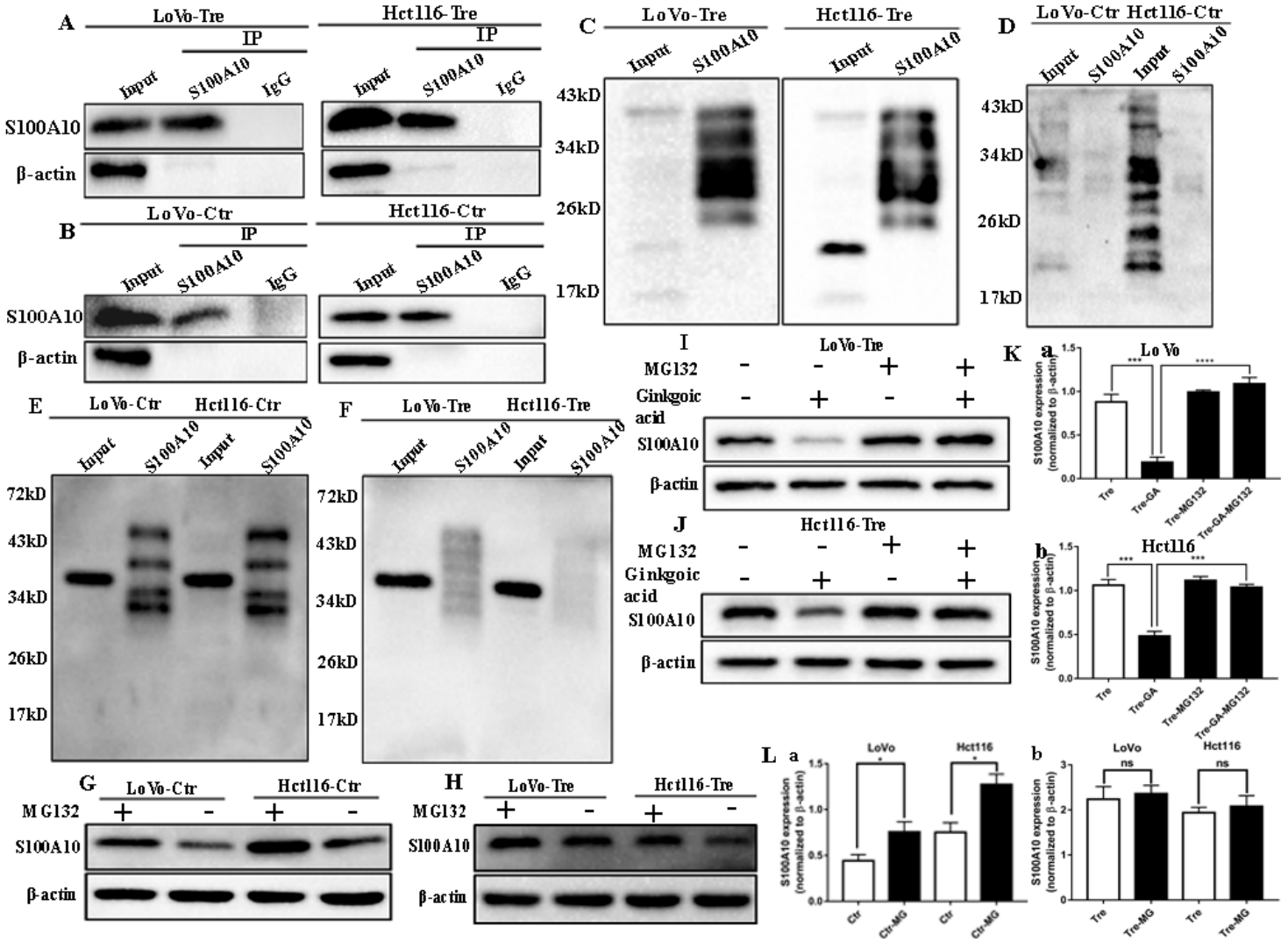

Figure 2

SUMOylation and ubiquitination of S100A10 in LoVo and Hct116 cells before and after CoCl2 treatment. A. Results of S100A10 co-immunoprecipitation in LoVo and Hct116 PGCCs with daughter cells. B. Results of S100A10 co-immunoprecipitation in LoVo and Hct116 control cells. C. Total lysates of LoVo and Hct116 PGCCs with daughter cells were immunoprecipitated with anti-S100A10 and immunoblotted with anti-SUMO1. D. Total lysates of LoVo and Hct116 control cells were immunoprecipitated with anti-S100A10 and immunoblotted with anti-SUMO1. E. Total lysates of LoVo and Hct116 control cells were

immunoprecipitated with anti-S100A10 and immunoblotted with anti-Ubiquitin (linkage-specific K48). F. Total lysates of LoVo and Hct116 PGCCs with daughter cells were immunoprecipitated with anti-S100A10 and immunoblotted with anti-Ubiquitin (linkage-specific K48). G. S100A10 expression in LoVo and Hct116 control cells before and after the MG132 treatment. H. S100A10 expression in LoVo and Hct116 PGCCs with their daughter cells before and after the MG132 treatment. I. S100A10 expression in LoVo PGCCs and daughter cells with and without GA, MG132, and both GA and MG132 treatment. J. S100A10 expression in Hct116 PGCCs and daughter cells with and without GA treatment, treatment of MG132 and treatment of both GA and MG132 respectively. K. (a) Comparison of S100A10 in LoVo PGCCs and daughter cells with non-treatment, treatment of GA, treatment of MG132 and treatment of both GA and MG132 respectively. (b) Comparison of S100A10 in Hct116 PGCCs and daughter cells with and without GA, MG132 and both GA and MG132 treatment. L. (a) Comparison of S100A10 in LoVo and Hct116 control cells before and after MG132 treatment. (b) Comparison of S100A10 in LoVo and Hct116 PGCCs and daughter cells before and after MG132 treatment. Ctr: control cells; Tre: cells treated with CoCl2

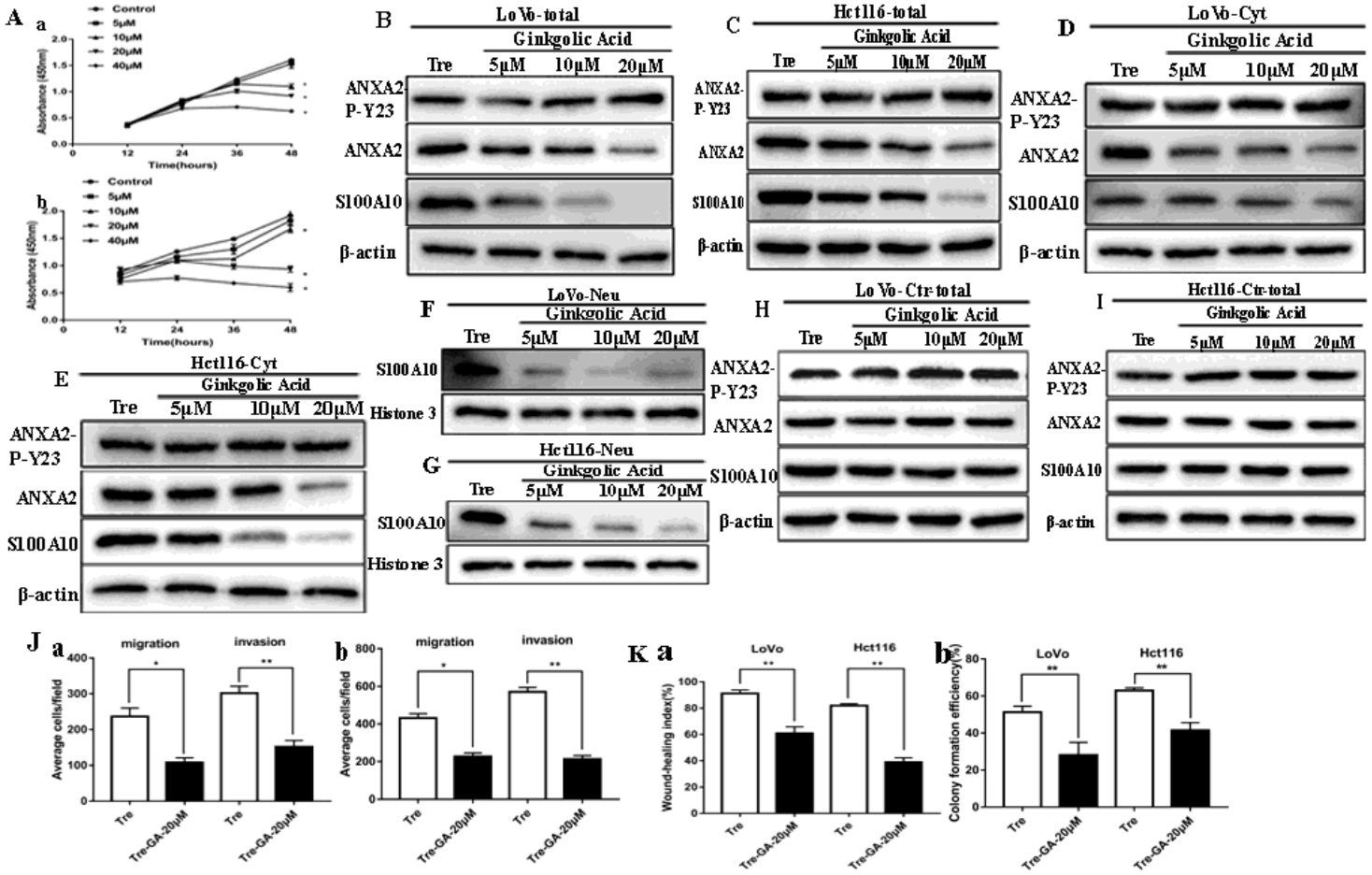

Figure 3

ANXA2-P-Y23, ANXA2, and S100A10 expression in LoVo and Hct116 PGCCs with daughter cells before and after GA treatment. A. Effects of GA on the viability of the PGCCs with their daughter cells derifed from LoVo and Hct116. Cells treated with 0 μM GA were used as a negative control group. Data are presented as the means±standard errors. *P<0.05 treatment vs. control group. (a) LoVo PGCCs with their daughter cells were treated with GA at different concentrations (0, 5, 10, 20, and 40 μM). At each time point (12, 24, 36, and 48 h), cell viability was assessed using CCK8 assay. (b) Hct116 PGCCs with their daughter cells were treated with GA at various concentrations (0, 5, 10, 20, and 40 μM). At each time point (12, 24, 36 and 48 h), cell viability was assessed using CCK8 assay. B. Total ANXA-P-Y23, ANXA2 and S100A10 expression in LoVo PGCCs with their daughter cells after GA treatment at 0, 5, 10, and 20 μM for 24 h. C. Total ANXA-P-Y23, ANXA2, and S100A10 expression in Hct116 PGCCs with their daughter cells after GA treatment at 0, 5, 10, and 20 μM for 24h. D. Cytoplasmic ANXA-P-Y23, ANXA2 and S100A10 expression in LoVo PGCCs with their daughter cells after GA treatment at 0, 5, 10, and 20 μM for 24 h. E. Cytoplasmic ANXA-P-Y23, ANXA2, and S100A10 expression in Hct116 PGCCs with their daughter cells after GA treatment at 0, 5, 10 and 20 μM, respectively for 24 h. F. Nuclear S100A10 expression in LoVo PGCCs with their daughter cells after GA treatment at 0, 5, 10, and 20 μM for 24 h. G. Nuclear S100A10 expression in Hct116 PGCCs with their daughter cells after GA treatment at 0, 5, 10, and 20 μM, respectively for 24 h. H. Total ANXA-P-Y23, ANXA2, and S100A10 expression in LoVo control cells after GA treatment at 0, 5, 10, and 20 μM for 24 h. I. Total ANXA-P-Y23, ANXA2, and S100A10 expression in Hct116 control cells after GA treatment at 0, 5, 10 and 20 μM for 24 h. J. (a) Comparison of the average cell number for migration and invasion assay in LoVo PGCCs and their daughter cells before and after 20 μM GA treatment for 24 h. (b) Comparison of the average cell number for migration and invasion assay in Hct116 PGCCs and their daughter cells before and after 20 μM GA treatment for 24 h. K. (a) Wound-healing index of LoVo and Hct116 PGCCs and their daughter cells before and after 20 μM GA treatment for 24 h. (b) Colony formation efficiency of LoVo and Hct116 PGCCs and their daughter cells before and after 20 μM GA treatment for 24 h. Tre: cells treated with $CoCl_2$; Cyt: cytoplasm; Neu: nucleus

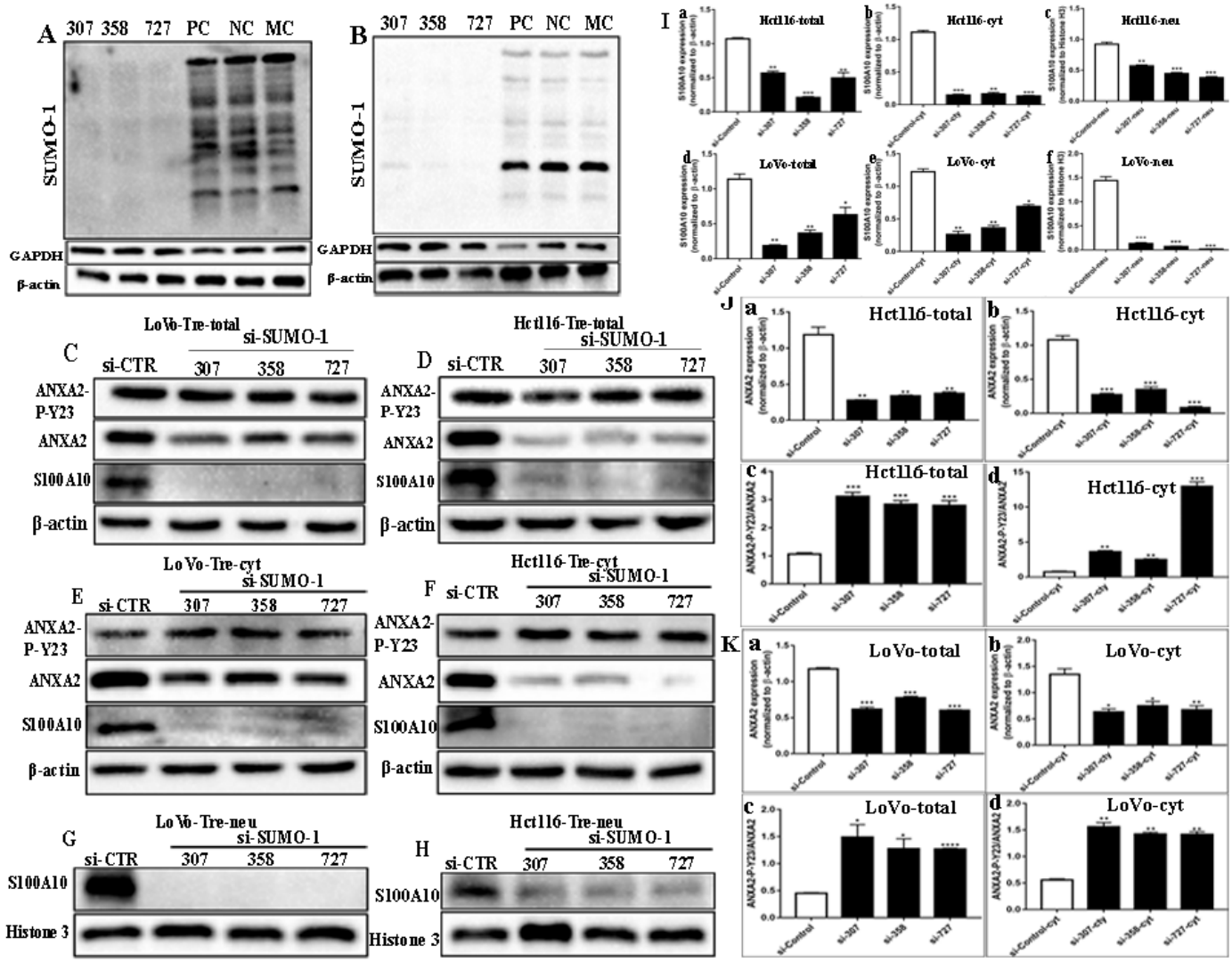

Figure 4

S100A10 and related protein expression in PGCCs with their daughter cells after siRNA SUMO1-207, 358, 727, siRNA control and negative control transfection. A. Total SUMO1 expression in LoVo PGCCs with their daughter cells. B. Total SUMO1 expression in Hct116 PGCCs with daughter cells. C. Total ANXA-P-Y23, ANXA2, and S100A10 expression in LoVo PGCCs with their daughter cells. D. Total ANXA-P-Y23, ANXA2, and S100A10 expression in Hct116 PGCCs with their daughter cells. E. Cytoplasmic ANXA2-P-Y23, ANXA2, and S100A10 expression in LoVo PGCCs with their daughter cells. F. Cytoplasmic ANXA2-P-Y23, ANXA2 and S100A10 expression in Hct116 PGCCs with their daughter cells. G. Nuclear S100A10 expression in LoVo PGCCs with their daughter cells. H. Nuclear S100A10 expression in Hct116 PGCCs with their daughter cells. I. Comparison of total S100A10 expression after transfection with siRNA SUMO1-307, 358, 727 and siRNA control. (a) Total S100A10 expression in Hct116 PGCCs and their daughter cells. (b) Cytoplasmic S100A10 expression in Hct116 PGCCs and their daughter cells. (c) Nuclear S100A10 expression in Hct116 PGCCs and their daughter cells. (d) Total S100A10 expression in LoVo PGCCs and their daughter cells. (e) Cytoplasmic S100A10 expression in LoVo PGCCs with their daughter cells. (f) Nuclear S100A10 expression in LoVo PGCCs with their daughter cells. J. Comparison

of total expression of ANXA2 after transfection with siRNA SUMO1-307, 358, 727 and siRNA control (a) Total expression of ANXA2 in Hct116 PGCCs with their daughter cells. (b) Cytoplasmic expression of ANXA2 in Hct116 PGCCs with their daughter cells. (c) Total expression of ANXA2-P-Y23 in Hct116 PGCCs with their daughter cells. (d) Cytoplasmic expression of ANXA2-P-Y23 in Hct116 PGCCs with their daughter cells. K. Comparison of total expression of ANXA2 after transfection with siRNA SUMO1-307, 358, 727 and siRNA control. (a) Total expression of ANXA2 in LoVo PGCCs with their daughter cells. (b) Cytoplasmic expression of ANXA2 in LoVo PGCCs with their daughter cells. (c) Total expression of ANXA2-P-Y23 in LoVo PGCCs with their daughter cells. (d) Cytoplasmic expression of ANXA2-P-Y23 in LoVo PGCCs with their daughter cells. Ctr: control cells; Tre: cells treated with CoCl2; Cyt: cytoplasm; Neu: nucleus

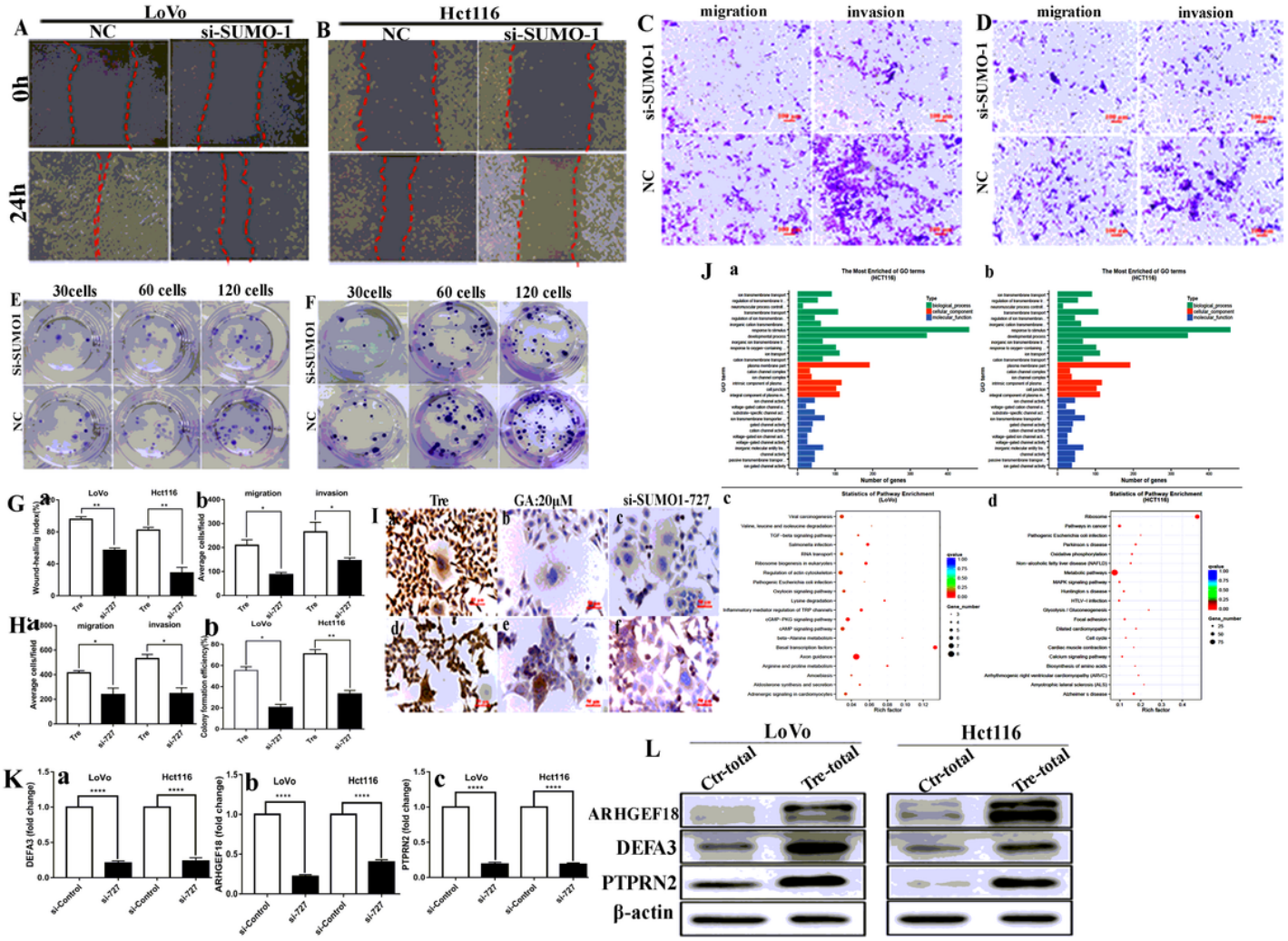

Figure 5

The motility, invasiveness and migration of LoVo and Hct116 PGCCs and daughter cells before and after SUMO1 knockdown and the results of ChIP-Seq and real-time PCR in these cells. A. Wound-healing assay in LoVo PGCCs with their daughter cells transfected with SUMO1-727 and control siRNAs. B. Wound-healing assay in Hct116 PGCCs with their daughter cells transfected with SUMO1-727 and control

siRNAs. C. The migration and invasion ability in LoVo PGCCs with their daughter cells transfected with SUMO1-727 and control siRNAs (100×). D. The migration and invasion ability in LoVo PGCCs with their daughter cells transfected with SUMO1-727 and control siRNAs (100×). E. Colony formation in LoVo PGCCs with their daughter cells transfected with SUMO1-727 and control siRNAs. F. Colony formation in Hct116 PGCCs with their daughter cells transfected with SUMO1-727 and control siRNAs. G. (a) Wound-healing index of LoVo and Hct116 PGCCs with daughter cells transfected with SUMO1-727 and control siRNAs. (b) Comparison of the average cell number for migration and invasion assay in LoVo PGCCs with daughter cells transfected with SUMO1-727 and control siRNAs. H. (a) Comparison of the average cell number for migration and invasion assay in Hct116 PGCCs with daughter cells transfected with SUMO1-727 and control siRNAs. (b) Colony formation efficiency in LoVo and Hct116 PGCCs with daughter cells transfected with SUMO1-727 and control siRNAs. I. ICC staining of S100A10 in the LoVo and Hct116 PGCCs with daughter cells (ICC, 400×). (a) ICC staining of S100A10 in LoVo PGCCs with daughter cells. (b) ICC staining of S100A10 in LoVo PGCCs with daughter cells after GA treatment at 20 μM. (c) ICC staining of S100A10 in LoVo PGCCs with daughter cells after SUMO1-siRNA 727 transfection. (d) ICC staining of S100A10 in Hct116 PGCCs with daughter cels. (b) ICC staining of S100A10 in Hct116 PGCCs with daughter cells after GA treatment at 20 μM. (c) ICC staining of S100A10 in Hct116 PGCCs with daughter cells after SUMO1-siRNA 727 transfection. J. (a) GO functional enrichment of targets associated with S100A10 in the PGCCs with daughter cells of LoVo ChIP-seq peaks for biological process. (b) GO functional enrichment of targets associated with S100A10 in the PGCCs with daughter cells of Hct116 ChIP-seq peaks for biological process. (c) KEGG pathway clustering analysis of targets associated with S100A10 in the PGCCs with daughter cells of LoVo ChIP-seq peaks. (d) KEGG pathway clustering analysis of targets associated with S100A10 in the PGCCs with daughter cells of Hct116 ChIP-seq peaks. K. Immunoprecipitated DNA before and after the knockdown of SUMO1 were analyzed using specific primers of DEFA3, ARHGEF18, and PTPRN2. (a) DEFA3, (b) ARHGEF18, (c) PTPRN2. L.The total ARHGEF18, DEFA3, and PTPRN2 expression in LoVo and Hct116 cells before and after CoCl2 treatment.

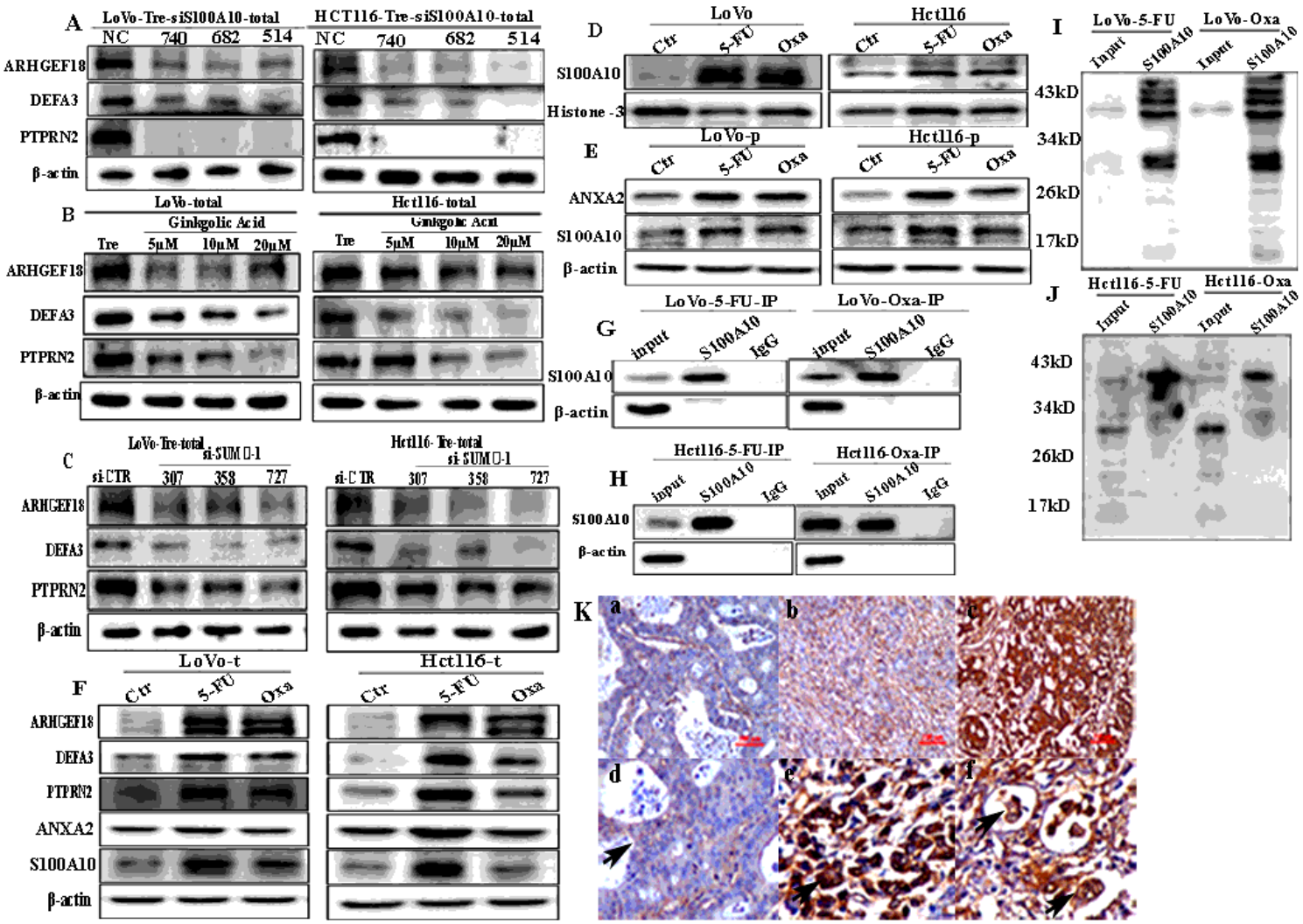

Figure 6

A. Total ARHGEF18, DEFA,3 and PTPRN2 expression in LoVo PGCCs with daughter cells after transfection with S100A10-740, 682, 514, siRNA control and negative control transfection. B. Total ARHGEF18, DEFA3, and PTPRN2 expression in LoVo and Hct116 PGCCs with their daughter cells after GA treatment at 0, 5, 10, and 20 μM for 24 h. C. C. Total ARHGEF18, DEFA3, and PTPRN2 expression in LoVo and Hct116 PGCCs with their daughter cells after siRNA SUMO1-207, 358, 727, siRNA control and negative control transfection. D. Nuclear S100A10 expression in LoVo and Hct116 cells before and after the treatment with 5-Fu and Oxa, respectively. E. Cytoplasmic ANXA2 and S100A10 expression in LoVo and Hct116 cells before and after the treatment with 5-Fu and Oxa, respectively. F. Total ANXA2, S100A10, ARHGEF18, DEFA3, and PTPRN2 expression in LoVo and Hct116 cells before and after the treatment with 5-Fu and Oxa, respectively. G. Results of S100A10 co-immunoprecipitation in LoVo cells after the treatment with 5-Fu and Oxa, respectively. H. Results of S100A10 co-immunoprecipitation in Hct116 cells after the treatment with 5-Fu and Oxa respectively. I. Total lysates of LoVo cells after the treatment with 5-Fu and Oxa were immunoprecipitated with anti-S100A10 and immunoblotted with anti-SUMO1, respectively. J. Total lysates of Hct116 cells after the treatment with 5-Fu and Oxa were immunoprecipitated with anti-

S100A10 and immunoblotted with anti-SUMO1, respectively. K. IHC staining of S100A10 in the human CRC tissues. (a) S100A10 expression in the well-differentiated CRC tissue (IHC, 200×). (b) S100A10 expression in the moderately differentiated CRC tissue (IHC, 200×). (c) S100A10 expression in the poorly differentiated CRC tissue (IHC, 200×). (d) Cytoplasmic expression of S100A10 in CRC cells (Black arrow heads, IHC, 400×). (e) Nuclear staining in cancer cells expressing S100A10 in CRC tissues (Black arrow heads, IHC, 400×). (d) Cytoplasmic and nuclear expression of S100A10 in PGCCs of CRC etissues (Black arrows head, IHC, 400×).

Supplementary Files

This is a list of supplementary files associated with this preprint. Click to download.

- Supplementarytable1.docx
- Supplementarytable2.docx
- Supplementarytable3.docx
- Supplementarytable4.docx
- supplementaryfigurelegends.doc
- supplementaryfigure1.tif
- supplementaryfigure2.tif
- supplementaryfigure3.tif
- supplementaryfigure4.tif
- supplementarymaterialsandmethods.docx